Journal of Materials Science & Technology 35 (2019) 1655–1661

Contents lists available at ScienceDirect

Journal of Materials Science & Technology

journal homepage: www.jmst.org

Research Article

Microstructure and soft-magnetic properties of FeCoPCCu nanocrystalline alloys

Long Hou[a,1], Xingdu Fan[a,1], Qianqian Wang[a], Weiming Yang[b], Baolong Shen[a,b,*]

[a] Jiangsu Key Laboratory for Advanced Metallic Materials, School of Materials Science and Engineering, Southeast University, Nanjing 211189, China
[b] Institute of Massive Amorphous Metal Science, China University of Mining and Technology, Xuzhou 221116, China

ARTICLE INFO

Article history:
Received 7 December 2018
Received in revised form 17 January 2019
Accepted 20 January 2019
Available online 15 March 2019

Keywords:
Anocrystalline alloy
Microstructure
Co addition
Soft-magnetic properties
Ferromagnetic exchange-coupling

ABSTRACT

$Fe_{83.2-x}Co_xP_{10}C_6Cu_{0.8}$ (x = 0, 4, 6, 8 and 10) alloys with a high amorphous-forming ability and good soft-magnetic properties were successfully synthesized. Saturation magnetic flux density (B_s) is effectively enhanced from 1.53 T to 1.61 T for as-quenched alloy by minor Co addition, which is consistent well with the result of the linear relationship between average magnetic moment and magnetic valence. For Co-contained alloys, the value of corecivity (H_c) is mainly determined by magneto-crystalline anisotropy, while effective permeability (μ_e) is dominated by grain size and average saturation polarization. After proper heat treatment, the $Fe_{79.2}Co_4P_{10}C_6Cu_{0.8}$ nanocrystalline alloy exhibited excellent soft-magnetic properties including a high B_s of 1.8 T, a low H_c of 6.6 A/m and a high μ_e of 15,510, which is closely related to the high volume fraction of α-(Fe, Co) grains and refined uniform nanocrystalline microstructure.

© 2019 Published by Elsevier Ltd on behalf of The editorial office of Journal of Materials Science & Technology.

1. Introduction

Fe-based nanocrystalline alloys with amorphous/crystalline composite structures have attracted great attention due to their excellent soft-magnetic properties such as high saturation magnetic flux density (B_s), low coercivity (H_c) and high effective permeability (μ_e) [1–3]. Among them, FeSiBNbCu (FINEMET) alloy has been widely used in electronic devices due to its high μ_e and low core loss [4,5]. However, the most commonly used FINEMET alloy exhibits a rather low B_s of only 1.24 T, which limits its industrial applications, as B_s is an important property in applications, the higher the B_s is, the smaller and more efficient the electronic devices can be made. Therefore, with the rapid development of modern electronics industry, it is important to develop nanocrystalline alloys with a higher B_s. For ferromagnetic soft magnetic alloys, the B_s is basically determined by ferromagnetic elements contents such as Fe, Co, and Ni, but non-ferromagnetic elements are also important for obtaining good magnetic softness, particularly, in some high entropy soft magnetic alloys [6]. The optimization of non-ferromagnetic elements is required to achieve an optimum combination of properties, especially to get the balance between mechanical and magnetic properties. For Fe-based amorphous/nanocrystalline alloys, the addition of non-ferromagnetic metalloid elements such as C [7,8], Si [9] and P [10,11] has been experimentally proved to favor amorphous formation, while metal elements such as Nb [12,13], Mn [14], Hf [15], and Mo [16,17] can inhibit the quick growth of nanocrystals due to their large atomic size and slow diffusion. Generally, a high Fe content is essential to achieve a high B_s, but an increase in the Fe content implies a decrease in non-ferromagnetic elements contents inside the alloy, leading to a series of problems such as the decrease of amorphous-forming ability (AFA), the decreasing thermal stability of residual amorphous phase, and the abnormal growth of crystalline grains, etc. Accordingly, how to achieve high B_s, high AFA and excellent soft-magnetic properties with high Fe content has always been a balance question in the study of nanocrystalline alloys.

Recently, by crystallizing hetero-amorphous phase, nanocrystalline FeSiBPCu alloy (NANOMET) has been developed with a B_s of >1.8 T, a low H_c of < 10 A/m, and especially a low core loss of 0.32 W/kg at 1.5 T and 50 Hz [18–20]. Moreover, this alloy also possesses low material cost as it does not contain noble metal elements. However, the relatively low AFA, by which the ribbon thickness is limited to 20 μm or less, constrains its application [18,19,21]. More recently, the FePCCu nanocrystalline alloys were successfully developed with good soft-magnetic properties including a relatively high B_s of 1.64–1.65 T, a low H_c of 3.3–3.9 A/m, and a high μ_e of 21000, respectively, as well as a higher AFA with 25 μm in

* Corresponding author at: Jiangsu Key Laboratory for Advanced Metallic Materials, School of Materials Science and Engineering, Southeast University, Nanjing 211189, China.
E-mail address: blshen@seu.edu.cn (B. Shen).
[1] Authors contributed equally to this work.

https://doi.org/10.1016/j.jmst.2019.03.030
1005-0302/© 2019 Published by Elsevier Ltd on behalf of The editorial office of Journal of Materials Science & Technology.

critical thickness [22,23]. However, the soft-magnetic properties, especially the B_s of these alloys, are still not comparable to those of the NANOMET alloy.

It has been reported that partial substitution of Co for Fe in Fe-based amorphous/nanocrystalline alloys is effective for AFA improvement and B_s tuning [21,24–27]. However, in some FeSiB-type alloys such as the FeSiBNbCu alloy, the AFA is significantly enhanced from ribbon to bulk glassy alloy with a diameter of 1.5 mm by 10 at.% Co addition [28], whereas the B_s does not increase, but exhibits a slight decrease instead. Similar results are also found in the FeSiBPCu alloys [29,30].

Therefore, with the aim of synthesizing novel alloys with high AFA without losing the B_s, the $Fe_{83.2-x}Co_xP_{10}C_6Cu_{0.8}$ (x = 0, 4, 6, 8 and 10) alloys have been developed. The amorphous formation, thermal stability and microstructure evolution of the FePCCu alloys with different amounts of Co substitution were investigated. The mechanism of Co addition on soft-magnetic properties especially the B_s was also discussed.

2. Experimental

Alloy ingots with nominal compositions of $Fe_{83.2-x}Co_xP_{10}C_6Cu_{0.8}$ (x = 0, 4, 6, 8 and 10) were prepared by induction melting the mixtures of pure Fe (99.99 mass%), Cu (99.995 mass%), Co (99.99 mass%), pre-alloyed Fe-P ingots (consisting of 75 mass% Fe and 25 mass% P) and Fe-C ingots (consisting of 96 mass% Fe and 4 mass% C) in an induction melting furnace under the protection of an argon atmosphere. Part of master alloy ingot was re-melted in a special quartz tube and then sprayed rapidly into the surface of a high-speed rotating single roller (roller speed 40 m/s, cavity pressure difference 0.015–0.02 MPa) to form as-quenched (AQ) ribbons. The width and thickness of ribbon samples are 1 mm and 22–28 μm, respectively.

Microstructure of ribbons was characterized by X-ray diffraction (XRD, Bruker D8 Discover diffractometer) with Cu $K\alpha_1$ radiation and transmission electron microscopy (TEM, JEM2000ex). Thermal parameters were measured by using a differential scanning calorimeter (DSC, NETZSCH 404 F3) under a flow of high purity argon with a heating rate of 0.67 K/s. AQ ribbons were cut into 6 mm and then isothermally annealed in the vacuum chamber to develop nanocrystalline alloys. The B_s and H_c were measured using a vibrating sample magnetometer (VSM, Lake Shore 7410) under an applied field of 800 kA/m, and a B-H loop tracer (RIKEN BHS-40) under a field of 1 kA/m, respectively; μ_e was measured by an impedance analyzer (Agilent 4294 A) under a field of 1 A/m. For all magnetic measurements, three specimens were measured for each alloy to ensure credible results.

3. Results

Fig. 1 shows the XRD patterns of free surface of the $Fe_{83.2-x}Co_xP_{10}C_6Cu_{0.8}$ (x = 0, 4, 6, 8 and 10) AQ ribbons. The Co-free alloy shows a small crystallization peak at $2\theta = 44.5^\circ$ which corresponds to the (110)-reflection of α-Fe crystalline phase, indicating a poor AFA. However, for the alloys with Co addition, only a typical broad diffraction feature without any detectable sharp peaks is observed, indicating the formation of amorphous structures. As a result, the addition of Co element can effectively improve the AFA of FePCCu alloys.

The thermal performance of the AQ ribbons was investigated by DSC, as shown in Fig. 2. Two exothermic peaks for each alloy can be easily observed, suggesting the crystallization proceeds in two stages. It was reported that the first exothermic peak corresponds to the crystallization of α-Fe phase while the second one corresponds to that of Fe_3P and Fe_3C compounds [22]. The onset

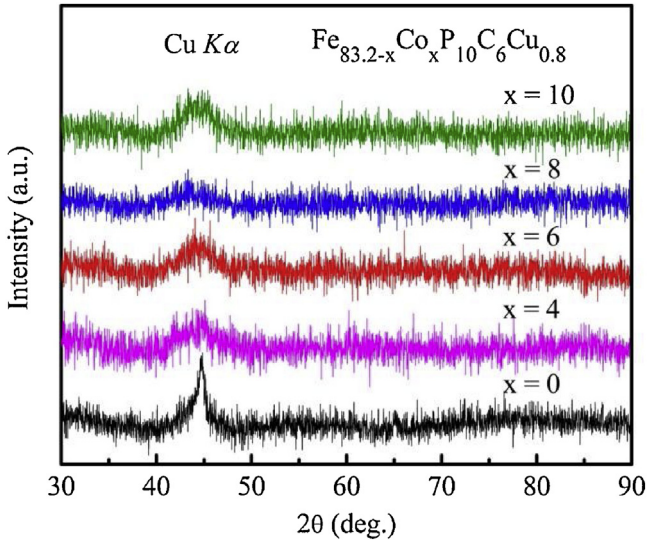

Fig. 1. XRD patterns of AQ $Fe_{83.2-x}Co_xP_{10}C_6Cu_{0.8}$ (x = 0, 4, 6, 8 and 10) alloy ribbons.

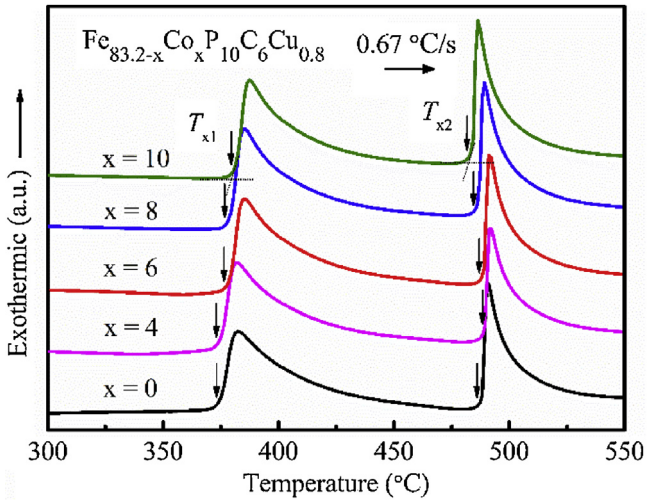

Fig. 2. DSC curves of AQ $Fe_{83.2-x}Co_xP_{10}C_6Cu_{0.8}$ (x = 0, 4, 6, 8 and 10) alloy ribbons with a heating rate of 0.67 °C/s.

temperature of the first crystallization (T_{x1}) has almost no change for the alloy with 4 at.% Co addition compared with that for Co-free alloy, while it increases slightly with further increase in Co to 10 at.%. Meanwhile, the second crystallization temperature (T_{x2}) increases slightly for alloy with 4 at.% Co, then decreases with further increase of Co to 10 at%. Accordingly, the temperature interval ($\Delta T_x = T_{x2} - T_{x1}$) is first slightly enlarged and then decreased as listed in Table 1. The large ΔT_x with minor Co substitution provides a wider crystallization window for the formation of α-(Fe, Co) phase without the second precipitation phases, which favors the achievement of good magnetic softness.

Fig. 3 shows the annealing temperature (T_a) dependence of H_c for $Fe_{83.2-x}Co_xP_{10}C_6Cu_{0.8}$ alloys. The inset is the variation curve of H_c with annealing time at 390 °C for $Fe_{79.2}Co_4P_{10}C_6Cu_{0.8}$ alloy, and this temperature is over T_{x1} to ensure the crystallization. Because the $Fe_{79.2}Co_4P_{10}C_6Cu_{0.8}$ alloy annealed for 2 min showed the lowest H_c, the optimum annealing time was determined to be 2 min for subsequently processed samples. As shown in Fig. 3, except for the Co-free alloy, all alloys exhibit a similar variation tendency, i.e. with increasing T_a from 350 to 470 °C, the values of H_c slightly decrease and then rise, followed by a distinct increase at 490 °C. The decrement of H_c of the alloy annealed below T_{x1} is mainly caused

Table 1
Thermal parameters and magnetic properties of $Fe_{83.2-x}Co_xP_{10}C_6Cu_{0.8}$ nanocrystalline alloys annealed at 470 °C for 2 min.

Alloys	Thermal parameters			Magnetic properties		
	T_{x1}(°C)	T_{x2}(°C)	ΔT_x(K)	B_s(T)	H_c(A/m)	μ_e(1 kHz)
$Fe_{83.2}P_{10}C_6Cu_{0.8}$	373	485	112	1.71	8.6	9910
$Fe_{79.2}Co_4P_{10}C_6Cu_{0.8}$	373	489	116	1.80	6.6	15,510
$Fe_{77.2}Co_6P_{10}C_6Cu_{0.8}$	376	487	111	1.77	15.3	4800
$Fe_{75.2}Co_8P_{10}C_6Cu_{0.8}$	376	485	109	1.75	19.1	4340
$Fe_{73.2}Co_{10}P_{10}C_6Cu_{0.8}$	380	483	103	1.74	44.9	5030
$Fe_{83.25}P_{10}C_6Cu_{0.75}$ [22]	384	491	107	1.65	3.3	21100
$Fe_{83.25}P_9C_7Cu_{0.75}$ [23]	385	490	105	1.64	3.9	21000

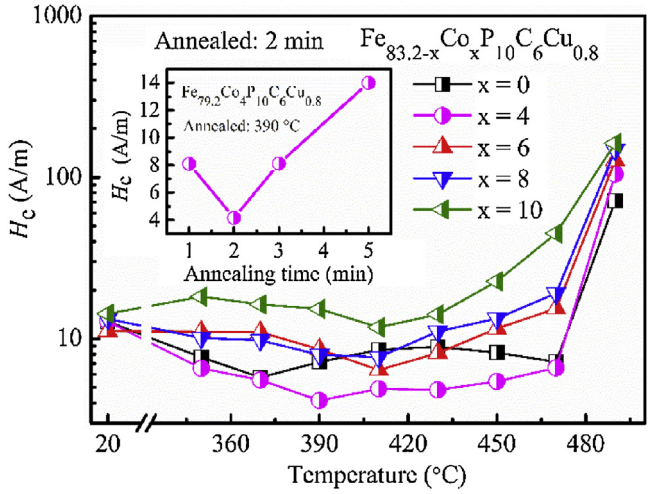

Fig. 3. Annealing temperatures (T_a) dependence of coercivity (H_c) for $Fe_{83.2-x}Co_xP_{10}C_6Cu_{0.8}$ (x = 0, 4, 6, 8 and 10) alloy ribbons, and the inset is the dependence of H_c on annealing time (t) for $Fe_{79.2}Co_4P_{10}C_6Cu_{0.8}$ alloy annealed at 390 °C.

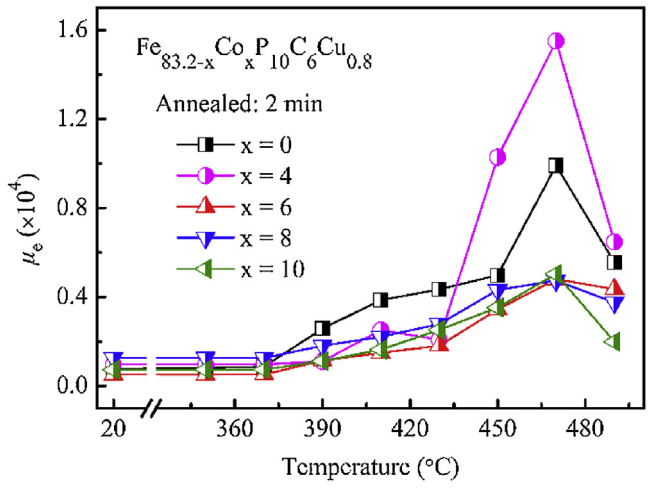

Fig. 4. Dependence of effective permeability (μ_e) on T_a for $Fe_{83.2-x}Co_xP_{10}C_6Cu_{0.8}$ alloy ribbons.

by internal stress relief and the uniformity of amorphous structure enhancement, but between T_{x1} and T_{x2} is attributed to the precipitation of α-(Fe, Co) phase. When T_a is near or higher than T_{x2}, the quick growth of α-(Fe, Co) grains and the precipitation of Fe_3P compound will greatly degrade the soft-magnetic properties. As for the alloy with no Co addition, the H_c is larger than that of the alloy with 4 at% Co, which is owed to the pre-existing α-Fe crystalline grains according to the XRD result. Meanwhile, there exists a slight increase in H_c before it rapidly increases due to the second inhomogeneous crystallization behavior. The T_a dependence of μ_e of $Fe_{83.2-x}Co_xP_{10}C_6Cu_{0.8}$ alloys was also investigated. As shown in Fig. 4, with the increase in T_a, μ_e firstly increases gradually and reaches its maximum at 470 °C and then obviously drops. Thus, the optimal annealing temperature is 470 °C, at which all alloys exhibit the maximum μ_e.

The magnetic performance and corresponding microstructure of FeCoPCCu alloys during the annealing process were analyzed. Here, we only investigated the typical $Fe_{83.2-x}Co_xP_{10}C_6Cu_{0.8}$ (x = 0, 4 and 10) alloys in detail. The T_a dependence of B_s of the $Fe_{83.2-x}Co_xP_{10}C_6Cu_{0.8}$ alloys is shown in Fig. 5(a). The value of B_s clearly increases from 1.53 T to 1.61 T for the AQ alloys with different Co addition, which can be attributed to the strong ferromagnetic exchange-coupling between Co and Fe [25,31]. During the annealing process, the B_s of all alloys increases with increase in T_a, and the alloy with 4 at% Co addition possesses the maximum B_s of 1.80 T at 470 °C and 1.81 T at 490 °C, respectively. Then, the microstructure evolution for $Fe_{79.2}Co_4P_{10}C_6Cu_{0.8}$ alloy annealed at different T_a was investigated by XRD, as shown in Fig. 5(b). When T_a is below 410 °C, only one sharp crystallization peak can be detected at 2θ = 44.5°, while annealed at 430 °C and above, three typical crystallization peaks of α-(Fe, Co) phase at 2θ = 44.5°, 64.5° and 82.3° can be detected. This indicates that α-(Fe, Co) phases are fully precipitated once the T_a reaches a certain value and finally, resulting in an increment of crystallization volume fraction (V_{cry}) of α-(Fe, Co) grains. For nanocrystalline alloys, the relationship between B_s and Vcry can be expressed as the following equation [32]:

$$B_s = B_{sc}V_{cry} + B_{sa}(1 - V_{cry}) \quad (1)$$

where B_{sc} and B_{sa} are the saturation magnetic flux densities of the crystalline and amorphous phases, respectively. Moreover, the B_{sc} (~2.1 T) is larger than B_{sa} (~1.5 T) of Fe-based amorphous alloys [33]. Therefore, B_s strongly depends on the Vcry. According to Fig. 5(b), with the increment of T_a, a large amount of α-(Fe, Co) nanocrystals precipitates from amorphous matrix, which gives rise to the V_{cry} of α-(Fe, Co) grains. The increment in the number density and V_{cry} promotes the exchange coupling between grains and thus leads to a rapid increase in B_s [31,34]. However, with the T_a up to 490 °C, although the B_s reaches a maximum value of 1.81 T due to the higher Vcry, the Fe_3P second crystalline phase is induced by high T_a, both the coarsening and growth of grains, and the precipitation of Fe_3P compound inevitably causing a deterioration of H_c. As a result, optimal soft-magnetic properties were obtained by annealing at 470 °C for 2 min, where the $Fe_{79.2}Co_4P_{10}C_6Cu_{0.8}$ nanocrystalline alloy exhibits a high B_s of 1.8 T, low H_c of 6.6 A/m and high μ_e of 15,510.

Fig. 5(c) shows the hysteresis loops of $Fe_{83.2-x}Co_xP_{10}C_6Cu_{0.8}$ alloys annealed at 470 °C for 2 min. With the substitution of Co, B_s increases firstly and then drops. The maximum value of B_s is achieved for the alloy with 4 at.% Co addition. Fig. 5(d) exhibits the microstructure change with Co content for the alloys annealed at optimal conditions (470 °C, 2 min). The alloy with 4 at.% Co shows a higher Vcry (~37%) compared to that of other alloys due to the high integral intensity of diffraction peak of α-(Fe, Co) (the calculation of V_{cry} is based on Ref. [35]). Thus, the high Vcry of α-(Fe,

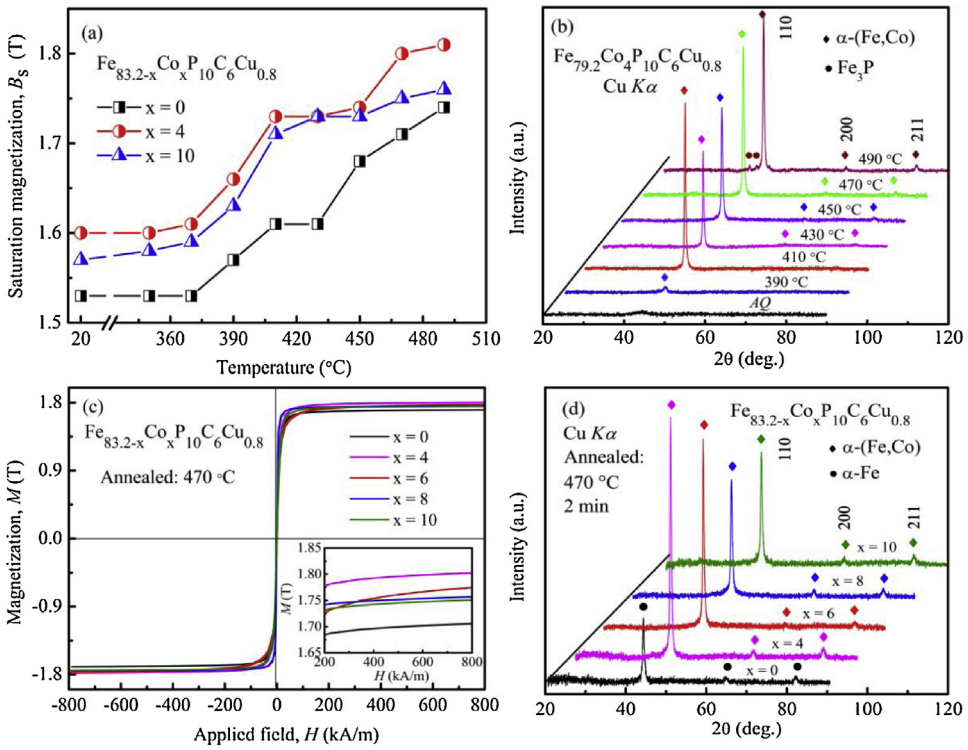

Fig. 5. Magnetization performance and microstructure evolution of FeCoPCCu alloys during the annealing process.

Co) grains leads to the high B_s. Except for the influence of Vcry, the B_{sc} of α-(Fe, Co) phase (≈2.45 T) is higher than that of α-Fe (≈2.1 T) [24,33]. Thus, compared to the Co-free alloy, B_s can be affected by synergetic influence of Vcry and B_{sc} for the alloys with Co addition.

As soft-magnetic properties are greatly dependent on structure, microstructure evolution of nanocrystalline alloys was further investigated by TEM. Fig. 6 shows the bright-field TEM images of $Fe_{83.2-x}Co_xP_{10}C_6Cu_{0.8}$ (x = 0 and 4) alloys under different annealing temperatures. As shown in Fig. 6(a), a small amount of nanocrystals can be observed in AQ Co-free alloy. The selected area electron diffraction (SAED) pattern (see the inset of Fig. 6(a)) also reveals the presence of crystalline grains, which is consistent well with the XRD measurement and forms a clear contrast with the AQ 4 at% Co-contained alloy, which only shows an amorphous structure feature [see Fig. 6(d)]. Fig. 6(b, c) and (e, f) show nanocrystalline microstructure of the Co-free and contained 4 at% alloys annealed at 410 °C and 470 °C for 2 min, respectively, in which the α-Fe/(Fe, Co) grains are randomly oriented in all the annealed samples according to the SAED patterns. Meanwhile, the average grain sizes (D) are ≈27 and 20 nm for the annealed 410 °C and 470 °C Co-free alloy and ≈24 and 18 nm for the Co-contained (4 at.%) alloy, respectively. This result indicates that, with the increase of T_a, both alloys exhibit grain refinement. Especially, the alloy with 4 at% Co represents a more uniform microstructure with much narrower grain distribution from 10 to 30 nm compared with the Co-free alloy, for which the α-Fe grains are distributed inhomogeneously due to the pre-existing α-Fe nanocrystals.

4. Discussion

In this study, it is found that Co addition effectively enhances the AFA and B_s of $Fe_{83.2-x}Co_xP_{10}C_6Cu_{0.8}$ alloys. Here, we firstly discuss the reasons for the improvement of AFA. When Co is added into the base alloy, the degree of ordering around local Fe and Co atoms could be increased due to the strong bonding nature among the constituent elements [36]. Former research suggests that there is a special chemical short-range order existing in the atomic structure of melting state for amorphous precursor, which can be characterized as the solute-centered atomic cluster in transition metal-metalloid amorphous alloys [37,38]. Therefore, Co addition could lead to a special P/C-centered atomic cluster, which effectively increases the density and viscosity of the molten liquid, thereby inhibiting the long-range diffusion of atoms [17] and finally improving the thermal stability and AFA of alloys. It should be noted that the Co-free alloy exhibits slight crystallization in this work, which seems to be inconsistent with our previous work [22]. The deterioration of AFA may be attributed to the thicker ribbon thickness and different purities of raw materials of the alloys.

Secondly, the increase of B_s by Co addition can be interpreted by the theory of strong ferromagnetism according to magnetic valence theory [31,39]. Based on this theory, the average magnetic valence of $\bar{V}_m$ can be expressed as $\bar{V}_m = \sum V_{m,i}X_i$, where X_i is the atomic fraction and $V_{m,i}$ is the magnetic valence of the ith element, respectively, with $V_m = 2N_d^{\uparrow} - Z$ ($N_d^{\uparrow}$ is the number of spin-up d-band electrons per atom and Z is chemical valence). The above theory is based on the strong ferromagnetism, i.e. $N_d^{\uparrow}$ for the magnetic elements (Fe, Co and Cu) and non-ferromagnetic elements (P and C) are 5 and 0, respectively. Therefore, the calculated V_m for Fe, Co, P, C and Cu atoms are 2, 1, −5, −4 and −1, respectively, and finally the $\bar{V}_m$ of the studied AQ alloys can be obtained. Meanwhile, the magnetic moment per magnetic atom (μ_m) can be calculated by using $\mu_m = V_M J_s/(N_A \mu_B)$, where V_M is the molar volume of ferromagnetic atom, J_s is the saturated magnetic polarization, N_A and μ_B denotes the Avogadro constant and Bohr magneton, respectively [40]. Accordingly, the relationship between μ_m and $\bar{V}_m$ can be obtained as shown in Fig. 7. As a result, the μ_m of the base alloy is extremely low while it can be significant strengthened by Co addition and exhibits a linear relationship to $\bar{V}_m$, and thus the deviation from linearity without Co addition implies that the Fe(Co)PCCu alloy undergoes a distinct transition behavior from weak ferromagnetism to strong ferromagnetism, which is similar to the previously work [38,39]. Moreover, based on the Bethe-Slater curve [34] (see

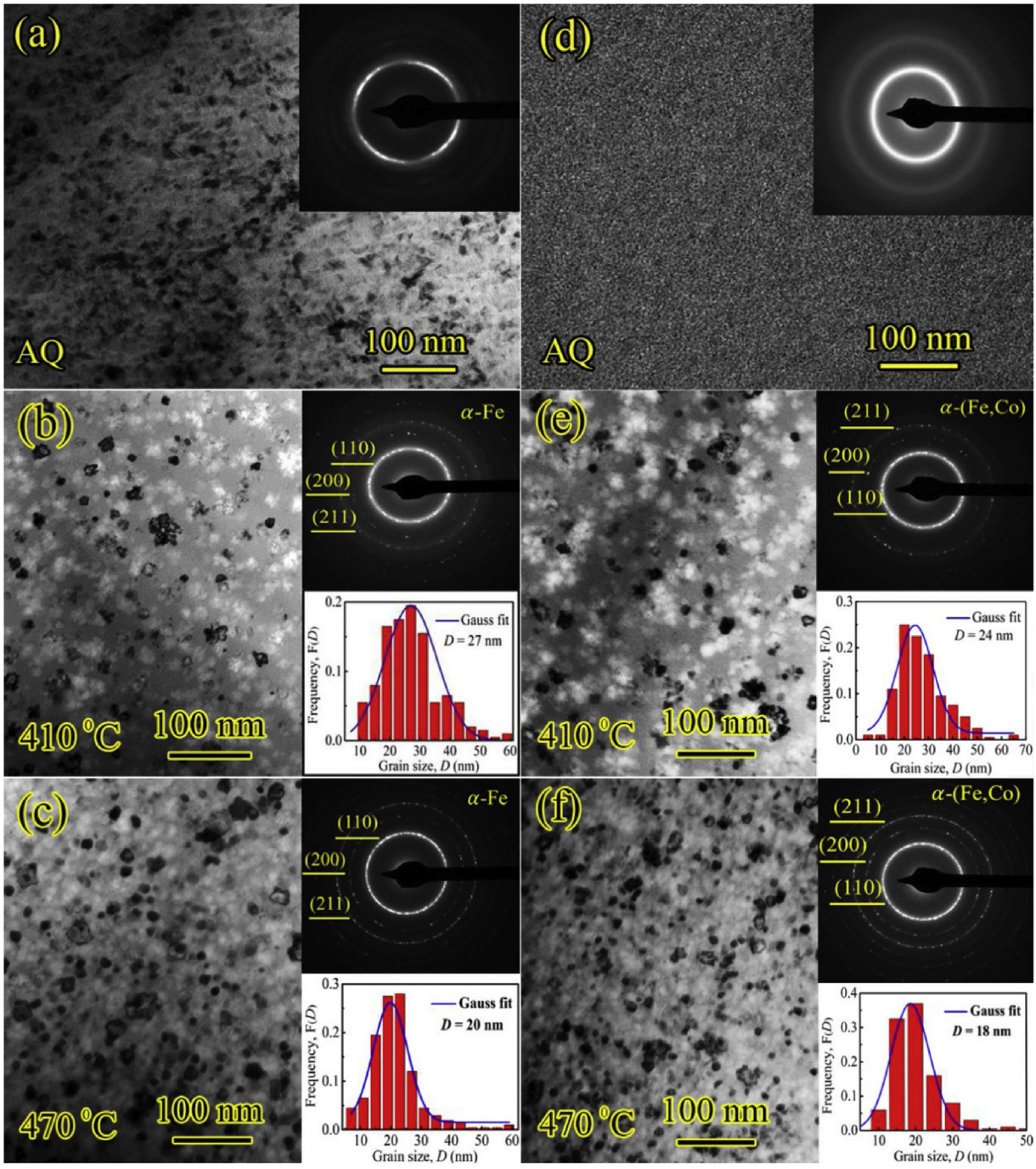

Fig. 6. Brigh-field TEM images of $Fe_{83.2-x}Co_xP_{10}C_6Cu_{0.8}$ alloys with x = 0 (a) AQ ribbons, (b) and (c) corresponding the ribbons annealed at 410 °C and 470 °C for 2 min, respectively; x = 4 (d) AQ ribbons, (e) and (f) corresponding the ribbons annealed at 410 °C and 470 °C for 2 min, respectively. The inset is the corresponding selected area electron diffraction (SAED) patterns and grain size distributions.

the inset of Fig. 7), there should exist an optimal value of r_{ab}/r_d (r_{ab} is the interatomic distance and r_d is the radius of an unfilled d-shell), where the strongest exchange interacting strength is achieved. For the $Fe_{83.2-x}Co_xP_{10}C_6Cu_{0.8}$ alloys, the optimal position may lie in the alloy with composition of x = 4, where it possesses the highest B_s. Noting that the effect of Co concentration on B_s also depends on alloy compositions, different alloy system may exhibit different variation trend of B_s towards Co concentration, such as in the NANOMET-type alloys [29,41], the B_s decreases only when the Co content is over 25 at.%, while in the FeCoPC alloy [42], the maximum B_s is achieved for the alloy with 5 at.% Co addition, which is similar to our work.

Thirdly, we discuss the abnormal variation of soft-magnetic properties towards microstructure for Co-contained nanocrystalline alloys. Here, the typical alloy with 4 at.% Co addition was also used for investigation. According to the XRD and TEM measurement, there is an obvious decrease in D due to the grain refinement with increasing T_a, but the H_c exhibits an increasing variation (see the light green area in Fig. 8(a)). The result seems to be contrary with Herzer's random anisotropy model [43], which points out that the value of H_c follows the D^6 proportional rule. The first reason is that the average D for 4 at.% Co-contained alloy is 18 nm, which may be larger than ferromagnetic exchange correlation length (L_{ex}, only 5–10 nm for Co-based alloy [44]). Secondly, the higher V_{cry} of α-

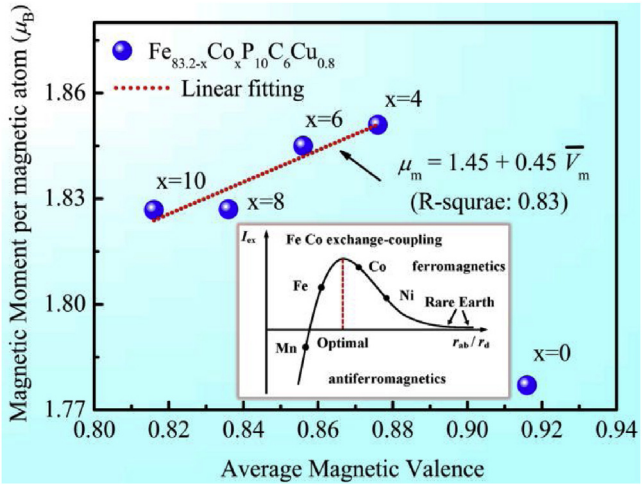

Fig. 7. Relationship between average magnetic moment and magnetic valence of AQ $Fe_{83.2-x}Co_xP_{10}C_6Cu_{0.8}$ alloys, the inset is the Bethe-Slater curve with the different elements.

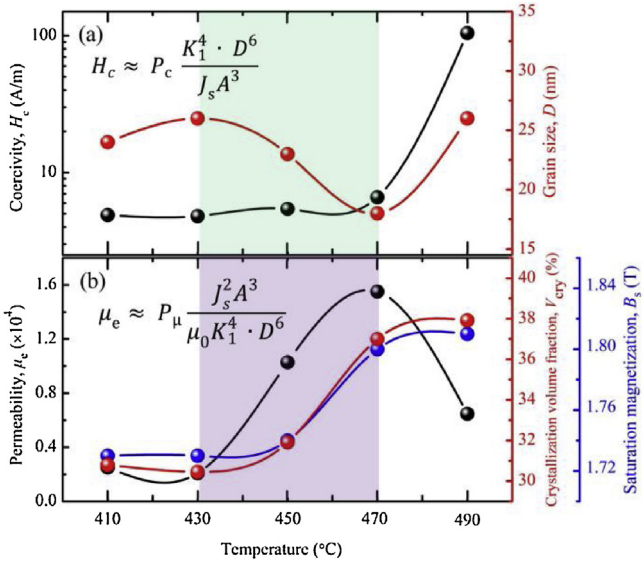

Fig. 8. (a) Change of coercivity (H_c) and grain size (D) with annealing temperature (T_a), (b) the variation trend of effective permeability (μ_e), crystallization volume fraction (V_{cry}) and saturation magnetization (B_s) dependent on T_a for $Fe_{79.2}Co_4P_{10}C_6Cu_{0.8}$ alloy.

(Fe, Co) grains also induces larger magneto-crystalline anisotropy (<K>) as the magneto-crystalline anisotropy constant of α-(Fe, Co) is greater than that of α-Fe [45]. Considering the above two factors, the ferromagnetic exchange-coupling interaction may not be too strong to effectively average out the large <K> in Co-contained alloy, hence leading to a larger H_c. As μ_e generally takes an opposite towards H_c, μ_e should be theoretically small when <K> is large. But, actually, there is a significant increase in μ_e before 470 °C, where large <K> is induced, indicating that <K> is not dominant. Fig. 8(b) shows the μ_e, V_{cry} and B_s dependent on T_a. It can be clearly seen that the variation of μ_e is quite in accordance with that of V_{cry} and B_s. Meanwhile, the variation tendency of μ_e is also consistent well with the opposite change of D. Accordingly, for the FeCoPCCu nanocrystalline alloys, it is believed that the value of μ_e is mainly affected by the average saturation polarization (J_s) and D, while the value of H_c is mainly determined by <K>.

Finally, the microstructure evolution of Fe(Co)PCCu alloys is summarized as illustrated in Fig. 9. There exist a few α-Fe nanocrystals embedded in amorphous matrix for Co-free alloy. Under heat treatment, except for the pre-existing α-Fe crystalline grains growth, a large number of new α-Fe grains are separated out and continuous to grow, leading to the slight increase in H_c. When annealed at a proper temperature (e.g. 470 °C), the maximum nucleation rate may occur, where the highest number density of nanocrystals with smallest D is formed, leading to a non-uniform refined nanocrystalline structure. On the contrary, the alloy with 4 at.% Co addition displays a typical amorphous structure in AQ state. It has been reported that the simultaneous additions of P and Cu to Fe-based alloys could induce some inhomogeneities, such as α-Fe nano-clusters during the quenching process, hence the separated Cu/P-Cu clusters might act as nucleation sites for α-Fe [46–48]. Although, in our work, it was not found due to its very small size and low V_{cry}, the influence of these clusters must be considered due to the large positive mixing enthalpy of 13 and 6 kJ/mol between Fe/Co and Cu atoms [36]. Thus, with Co addition, the primary crystallization phase changes from α-Fe to α-Fe and α-(Fe, Co) combined phases. The competing formation of different phases is beneficial for the AFA. Meanwhile, with the increase in T_a, the nucleation, growth and interaction of α-(Fe, Co) grains adhering to Cu/P-Cu clusters leads to a more uniform nanostructure with a higher number density of nanocrystals. As listed in Table 1, compared to the reported nanocrystalline $Fe_{83.25}P_{10}C_6Cu_{0.75}$ [22] and $Fe_{83.25}P_9C_7Cu_{0.75}$ [23] alloys, the B_s is significantly enhanced from 1.65 T to 1.74–1.8 T, which promises the application at higher excitation magnetic field. Meanwhile, the $Fe_{79.2}Co_4P_{10}C_6Cu_{0.8}$ nanocrystalline alloy annealed at proper condition also combines with a relative low H_c of 6.6 A/m and high μ_e of 15,510. The present work reveals the mechanism of Co addition on tuning AFA and soft-magnetic properties of FeCoPCCu alloys, and promotes the potential application as magnetic functional materials.

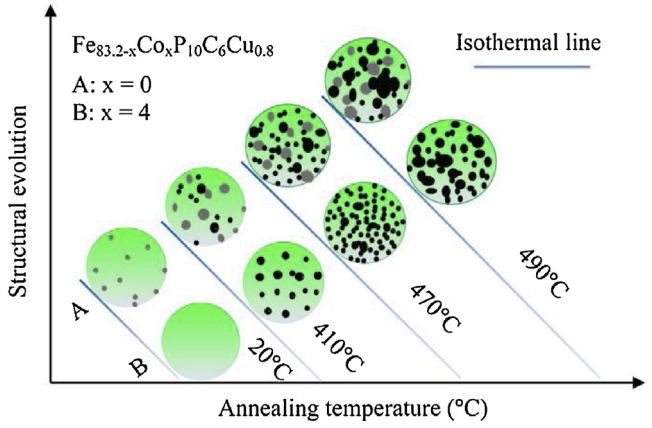

Fig. 9. Sketch map of microstructure evolution of the AQ alloys with x = 0 (A) and x = 4 (B) at different T_a.

5. Conclusion

In this work, $Fe_{83.2-x}Co_xP_{10}C_6Cu_{0.8}$ (x = 0, 4, 6, 8 and 10) alloys with good soft-magnetic properties and higher AFA were obtained. The soft-magnetic properties towards microstructure evolution of FeCoPCCu alloys were investigated. It is found that H_c of Co-contained alloys exhibit different variation compared with that of Co-free alloy. For Co-contained alloys, H_c is mainly determined by <K> while μ_e is dominated by both D and J_s. The value of B_s is effectively enhanced for both amorphous and nanocrystalline alloys with proper Co addition. Due to the high V_{cry} of α-(Fe, Co) grains and refined uniform nanocrystalline microstructure, the $Fe_{79.2}Co_4P_{10}C_6Cu_{0.8}$ alloy annealed at 470 °C for 2 min was success-

fully developed combined with high B_s of 1.8 T, low H_c of 6.6 A/m and high μ_e of 15,510.

Acknowledgments

This work was supported by the National Key Research and Development Program of China (Grant No. 2016YFB0300502) and the National Natural Science Foundation of China (Grant Nos. 51631003, 51401052, 51871237 and 51501037).

References

[1] Y. Yoshizawa, S. Oguma, K. Yamauchi, J. Appl. Phys. 64 (1988) 6044–6046.
[2] K. Suzuki, A. Makino, A. Inoue, T. Masumoto, J. Appl. Phys. 70 (1998) 6232–6237.
[3] M.A. Willard, D.E. Laughlin, M.E. Mchenry, D. Thoma, K. Sickafus, J.O. Cross, V.G. Harris, J. Appl. Phys. 84 (1998) 6773–6777.
[4] M.E. McHenry, M.A. Willard, D.E. Laughlin, Prog. Mater. Sci. 44 (1999) 291–433.
[5] J. Petzold, Scripta Mater. 48 (2003) 895–901.
[6] T.T. Zuo, R.B. Li, X.J. Ren, Y. Zhang, J. Mag. Magn. Mater. 371 (2014) 60–68.
[7] J. Xu, Y.Z. Yang, W. Li, Z.W. Xie, X.C. Chen, J. Alloys. Compd. 727 (2017) 610–615.
[8] X.D. Fan, T. Zhang, M.F. Jiang, W.M. Yang, B.L. Shen, J. Non-Cryst. Solids 503–504 (2019) 36–43.
[9] J. Xu, Y.Z. Yang, W. Li, Z.W. Xie, X.C. Chen, Mater. Res. Bull. 97 (2017) 452–456.
[10] R.K. Roy, S. Shen, S.J. Kernion, M.E. Mchenry,J. Appl. Phys. 111 (2012), 07A301.
[11] C.J. Wang, A. He, A.D. Wang, J. Pang, X.F. Liang, Q.F. Li, C.T. Chang, K.Q. Qiu, X.M. Wang, Intermetallics 84 (2017) 142–147.
[12] A.D. Wang, M.X. Zhang, J.H. Zhang, H. Men, B.L. Shen, S.J. Pang, T. Zhang, J. Alloys. Compd. 536 (2012) S354–S358.
[13] Z. Xiang, A.D. Wang, C.L. Zhao, H. Men, X.M. Wang, C.T. Chang, D. Pan, J. Alloys. Compd. 622 (2015) 1000–1004.
[14] X.J. Jia, Y.H. Li, L. Wu, W. Zhang, AIP Adv. 8 (2018) 056110.
[15] L. Zhou, G.T. Wang, L.B. Zheng, Y.Z. Yang, J. Supercond. Nov. Magn. (2018) 1–6.
[16] J.F. Li, X. Liu, S.F. Zhao, H.Y. Ding, K.F. Yao, J. Mag. Magn. Mater. 386 (2015) 107–110.
[17] X.J. Jia, Y.H. Li, G. Xie, T. Qi, W. Zhang, J. Non-Crystal. Solids. 481 (2018) 590–593.
[18] A. Makino, H. Men, T. Kubota, K. Yubuta, A. Inoue, Mater. Trans. JIM 50 (2009) 204–209.
[19] A. Makino, H. Men, T. Kubota, K. Yubuta, A. Inoue, IEEE Trans. Magn. 45 (2009) 4302–4305.
[20] A. Makino, T. Kubota, K. Yubuta, A. Inoue, A. Urata, H. Matsumoto, S. Yoshida, J. Appl. Phys. 109 (2011) 07A302.
[21] A.D. Setyawan, K. Takenaka, P. Sharma, M. Nishijima, N. Nishiyama, A. Makino, J. Appl. Phys. 117 (2015) 17B715.
[22] Y.L. Jin, X.D. Fan, M. He, X.C. Liu, B.L. Shen, Sci. China Technol. Sci. 55 (2012) 3419–3424.
[23] R. Xiang, S.X. Zhou, B.S. Dong, G.Q. Zhang, Z.Z. Li, Y.G. Wang, J. Mater. Sci: Mater. Electron. 25 (2014) 2979–2984.
[24] Y. Zhang, P. Sharma, A. Makino, IEEE Trans. Magn. 50 (2014) 1–4.
[25] L. Xue, W.M. Yang, H.S. Liu, H. Men, A.D. Wang, C.T. Chang, B.L. Shen, J. Mag. Magn. Mater. 419 (2016) 198–201.
[26] Z.G. Shi, R. Li, T. Zhang, J. Alloys. Compd. 778 (2019) 302–308.
[27] P.B. Chen, T. Liu, F.Y. Kong, A.D. Wang, C.Y. Yu, G. Wang, C.T. Chang, X.M. Wang, J. Mater. Sci. Technol. 34 (2018) 793–798.
[28] A. Inoue, B.L. Shen, J. Mater. Res. 18 (2003) 2799–2806.
[29] K. Takenaka, A.D. Setyawan, Y. Zhang, P. Sharma, N. Nishiyama, A. Makino, Mater. Tran. JIM 56 (2015) 372–376.
[30] N. Nishiyama, K. Tanimoto, A. Makino, AIP Adv. 6 (2016) 055925.
[31] A. Williams, V. Moruzzi, A. Malozemoff, K. Terakura, IEEE Trans. Magn. 19 (1983) 1983–1988.
[32] G. Herzer, IEEE Trans. Magn. 25 (1989) 3327–3329.
[33] M. Ohta, Y. Yoshizawa, Appl. Phys. Lett. 91 (2007) 062517.
[34] R.E. Hummel, Electronic Properties of Materials, fourth edition, Springer Pub., 2011.
[35] A.G. Ilinsky, V.V. Maslov, V.K. Nozenko, A.P. Brovko, J. Mater. Sci. 35 (2000) 4495–4500.
[36] A. Takeuchi, A. Inoue, Mater. Trans. 46 (2005) 2817–2829.
[37] D.B. Miracle, Acta Mater. 54 (2006) 4317–4336.
[38] S.Y. Meng, H.B.Ling Q. Li, J.J. Zhang, Scripta Mater. 81 (2014) 24–27.
[39] S. Bhattacharya, E.A. Lass, S.J. Poon, G.J. Shiflet, M. Rawlings, M. Daniil, M.A. Willard, J. Appl. Phys. 111 (2012) 063906.
[40] L. Zhu, Y. Meng, X.B. Zhai, Y.G. Wang, S. Lan, J. Mag. Magn. Mater. 472 (2019) 49–52.
[41] M. Kuhnt, X.D. Xu, M. Amalraj, P. Kozikowski, K.G. Pradeep, T. Ohkubo, M. Marsilius, T. Strache, C. Polak, M. Ohnuma, K. Hono, G. Herzer, J. Alloys. Compd. 766 (2018) 686–693.
[42] K. Xu, H.B. Ling, Q. Li, J.F. Li, K.F. Yao, S.F. Guo, Intermetallics 51 (2014) 53–58.
[43] G. Herzer, IEEE Trans. Magn. 26 (1990) 1397–1402.
[44] K. Suzuki, G. Herzer, Scripta Mater. 67 (2012) 548–553.
[45] S. Chikazumi, Physics of Ferromagnetism, Oxford Sci. Pub., 2009.
[46] A. Makino, M. Bingo, T. Bitoh, K. Yubuta, J. Appl. Phys. 101 (2007) 09N117.
[47] X. Li, H. Kato, K. Yubuta, A. Makino, A. Inoue, Mater. Sci. Eng. A 527 (2010) 2598–2602.
[48] A. Makino, IEEE Trans. Magn. 48 (2012) 1331–1335.